Design of arbitrary optical filters in silicon-on-insulator using evanescently-coupled Bragg gratings

Daniel PEREIRA-MARTÍN [(1)], Alejandro ORTEGA-MOÑUX [(1)], Íñigo MOLINA-FERNÁNDEZ [(1)], José Manuel LUQUE-GONZÁLEZ [(1)], Pavel CHEBEN [(2)], Jens H. SCHMID [(2)], Winnie N. YE [(3)], Jiří ČTYROKÝ [(4)], J. Gonzalo WANGÜEMERT-PÉREZ [(1)]

1. Dpto. de Ingeniería de Comunicaciones, ETSI Telecomunicación, Universidad de Málaga, Campus de Teatinos s/n, 29071, Málaga, Spain
2. National Research Council Canada, 1200 Montreal Road, Bldg. M50, Ottawa, K1A 0R6, Canada
3. Department of Electronics, Carleton University, 1125 Colonel by Dr., Ottawa, Canada
4. Institute of Photonics and Electronics, CAS, Chaberská 57, 182 51 Prague, Czech Republic

Contact name: Daniel Pereira-Martín (dpm@ic.uma.es).

ABSTRACT:

Spectral filters are experiencing an increasing demand in several applications of the silicon-on-insulator (SOI) platform. Many works have demonstrated that arbitrary frequency responses can be synthesized by apodizing the coupling coefficient profile of an integrated Bragg grating. However, the high index contrast of the SOI platform hinders their practical implementation, due to the difficulty of achieving the precise control required in the Bragg strength. In this paper, we propose the implementation of spectral filters using an architecture based on placing loading segments within the evanescent field region of a photonic wire waveguide. The Bragg coupling coefficient can be accurately controlled by simply moving the segments away from, or closer to, the waveguide core. The layer-peeling algorithm, in conjunction with a Floquet-Bloch modal analysis, allows to determine the spatial distribution of the segments that synthesizes the desired spectrum. The proposed topology is verified by designing a filter with five arbitrary passbands.

Key words: Spectral filters, Silicon-on-insulator, Bragg gratings, layer-peeling.

1.- Introduction

Silicon-on-insulator (SOI) is the dominant platform for the development of photonic integrated circuits in silicon photonics. The use of CMOS manufacturing processes remarkably reduces the cost of these devices. Furthermore, the high refractive index contrast between silicon (n_{Si}=3.476) and silicon dioxide (n_{SiO2}=1.444) permits a high level of integration inside these chips. As a result of these advantages, SOI-based devices are becoming a recognized point of interest in several areas, such as next-generation communications systems, data interconnects, high-performance computing or sensing, among others [1].

A fundamental building block for many applications are the spectral filters, required in the design of DWDM systems [2], optical signal processing [3] or ultrafast pulse shaping [4], for example. In fiber optics, this type of filters can be implemented in a straightforward way by introducing a periodic variation in the refractive index profile (Fiber Bragg Gratings, FBG) [5]. These refractive index perturbations act reflecting a specific range of wavelengths and transmitting the rest. By properly apodizing the strength of the perturbation along the fiber, a filter with a desired target spectrum can be designed [6]. However, the implementation of Bragg gratings on SOI waveguides is far more complex. Firstly, in contrast to fiber optics,

the refractive indices of the used materials are hardly adjustable during the fabrication process. Secondly, the high index contrast of the SOI platform makes the accurate filter design challenging.

Several approaches to design Bragg gratings on SOI waveguides can be found in the literature. The most common is to introduce a periodic sidewall corrugation in a photonic wire waveguide [7]. The main disadvantage of this architecture is that it requires corrugations of only a few nanometers if sub-nanometers bandwidths are required, hereby giving rise to minimum feature sizes (MFS) so small that the filter performance may be compromised. The required MFS can be slightly relaxed by using waveguides with two etch steps (rib waveguides) instead of one (photonic wire waveguides), since it decreases the modal confinement and, therefore, the sensibility of the perturbation strength to the corrugation [8]. Some techniques based on changing the relative phase of the corrugations instead of its amplitude have been proposed in [9] and have been used to experimentally demonstrate apodized filters with complex spectral responses, such as Hilbert transformers [10] or multichannel filters [11].

Other possibility to implement Bragg gratings on SOI waveguides consists in placing silicon loading segments, next to a photonic wire waveguide, along the propagation direction (z) [12], as shown in Fig. 1. These segments interact with the evanescent part of the guided mode, and by simply modifying their distance to the central waveguide, the perturbation strength can be accurately controlled without reducing the required MFS. In addition, if the photonic wire waveguide is replaced by a subwavelength grating, i.e., a periodic waveguide whose period is shorter than half wavelength, the guided mode can be more delocalized, and the fabrication tolerance with respect to errors in the position and the size of the segments can be increased [13]. The operation of these filters has been recently demonstrated in [14], with experimental bandwidths ranging from 8 nm to 150 pm. However, this architecture has not yet been used to implement apodized filters with arbitrary spectral responses.

In this work, we specifically propose the usage of this topology (Fig. 1) to synthesize Bragg grating filters with any desired spectrum. The apodization profile required in both the gap between the central waveguide and the loading segments (g_k) and the distance between two consecutive segments (d_k) can be found by conveniently using the layer-peeling algorithm proposed in [6], in conjunction with a Floquet-Bloch electromagnetic analysis of a basic Bragg cell (one period) for different gap values. The proposed approach has been tested by designing a filter with five passbands at arbitrary wavelengths, achieving a good level of agreement between simulation results and initial target.

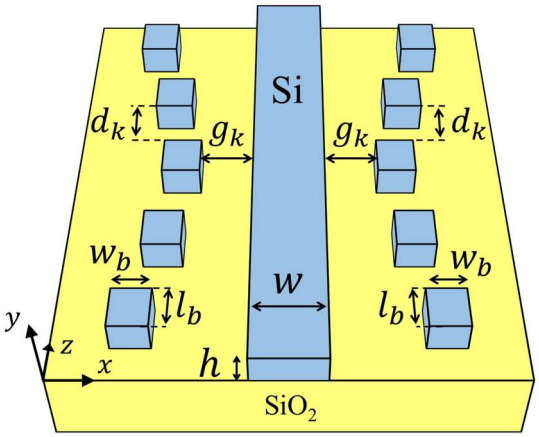

Fig. 1: Schematic representation of the structure proposed to synthesize filters with an arbitrary spectral response. The SiO_2 cladding is not shown for clarity.

2.- Analysis of Bragg gratings

2.1.- Coupled Mode Theory

The operation of Bragg gratings can be analyzed using the well-known Coupled Mode Theory (CMT) [15], which describes the field propagation along the grating by means of the forward and backward modes of a reference unperturbed waveguide (in our case, the central waveguide shown in Fig. 1). From the CMT, it is possible to determine that the (power) reflectance of the Bragg structure with respect to the operating wavelength λ is:

$$R(\lambda) = \frac{\kappa^2 \sinh^2[\sigma(\lambda) \cdot L]}{\sigma^2(\lambda) + \kappa^2 \sinh^2[\sigma(\lambda) \cdot L]}, \qquad (1)$$

κ is the coupling coefficient or Bragg strength, L is the total grating length,

$$\sigma(\lambda) = \sqrt{\kappa^2 - \delta^2(\lambda)}, \qquad (2)$$

and

$$\delta(\lambda = \lambda_B + \Delta\lambda) \approx -2\pi n_g \Delta\lambda/\lambda_B^2, \qquad (3)$$

where n_g is the group index of the unperturbed waveguide. As can be seen, the grating has a spectral response symmetric with respect to the Bragg wavelength λ_B. At this wavelength, the Bragg reflection coefficient reaches its maximum:

$$|\rho_{\max}| = \tanh(\kappa \cdot L). \qquad (4)$$

However, if the grating is considered short enough, it can be demonstrated that the reflection coefficient achieved for different wavelengths can be approximated by a constant value, given by Eq. 4. In this case, a Bragg grating behaves as a simple reflector rather than a spectral filter. This is a key point for the layer-peeling algorithm described in section 3.

2.2.- Characterization of the coupling coefficient: Floquet modal analysis

According to Eq. 4, the grating reflectivity can be controlled through the Bragg coupling coefficient κ. The calculation of this parameter can be carried out in two different ways. The first one is based on the analytical expressions derived from the CMT, which use the fields of the unperturbed waveguide and the corresponding refractive index perturbation introduced by the periodic structure. The second way consists in performing an electromagnetic simulation of only one Bragg period, imposing periodic boundary conditions and calculating the Floquet modes supported by the periodic structure. In this case, the coupling coefficient can be directly calculated as the maximum of the wavelength response of the Floquet mode attenuation constant α_F, obtained just for $\lambda = \lambda_B$, that is:

$$\kappa = \max\{\alpha_F(\lambda)\} = \alpha_F(\lambda_B). \qquad (5)$$

The Bragg cell to be characterized here is represented in Fig. 2(a). The height and the width of the central waveguide are, respectively, $h = 220$ nm and $w = 400$ nm, and the loading segments have a size of w_B x l_B = 200 nm x 215 nm. The polarization to be used is TM. The gap between the central waveguide and the segments is denoted by g, whereas the period size is Λ. Simplifying the 3D problem to be analyzed into a 2D equivalent problem by means of the Effective Index Method (EIM) [15], and using our 2D in-house simulation tool optimized for working with periodic structures [16], it is possible to efficiently compute the Floquet mode for a specific wavelength λ. To this end, we first calculated α_F for different wavelengths λ and different gaps g using a fixed period $\Lambda = 430$ nm (Fig. 2(b)). From these curves, it can

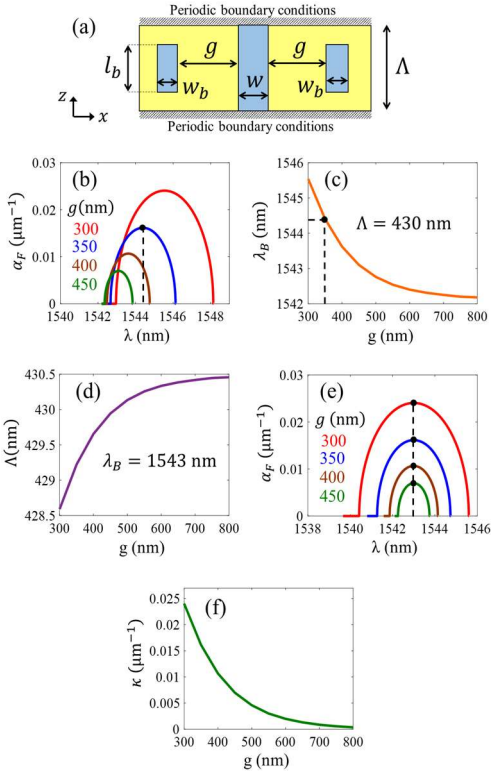

Fig. 2: (a) Schematic representation of the Bragg period to be analyzed. (b) Wavelength response of the Floquet attenuation constant for different gaps and maintaining the period equal to a fixed value ($\Lambda = 430$ nm) c) Variation of the Bragg wavelength as a function of the gap when maintaining the period equal to the same value. (d) Period size that must be used to keep the Bragg wavelength always to the same value ($\lambda_B = 1543$ nm). (e) Wavelength response of the Floquet attenuation constant for different gaps when changing the period accordingly to the values shown in (d). (f) Resultant coupling coefficient as a function of the gap.

be observed that, for different gaps, the Bragg wavelength λ_B, i.e., the point where α_F is maximum, slightly changes (Fig. 2(c)). Nevertheless, one of the conditions for the synthesis process to be described is just that the λ_B must remain unaltered. To overcome this issue, we have calculated what values of Λ should be used to keep λ_B changeless when varying g (Fig. 2(d)). Modifying the period accordingly, we recalculated the curves of α_F with λ (Fig. 2(e)). Now it can be seen that the value of λ_B is always the same. Finally, we calculated the coupling coefficient for different gaps by applying Eq. 5 (Fig. 2(f)).

3.- Synthesis technique: layer-peeling

Consider a structure conformed by cascading N single 1-period Bragg gratings. According to the model represented in Fig. 3, each grating is replaced by a discrete reflector, with a reflection coefficient provided by Eq. 4, and a transmission line whose electrical length is:

$$\theta(\lambda) = \beta_F(\lambda) \cdot \Lambda. \qquad (6)$$

β_F is the Floquet mode propagation constant and $\theta = \pi$ when $\lambda = \lambda_B$ (Bragg condition).

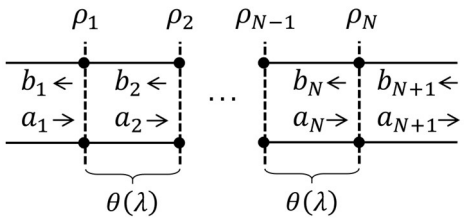

Fig. 3: Representation of the discrete model of reflectors and transmission lines used by the layer-peeling algorithm.

In this discrete model, a_k and b_k denote the complex amplitudes of the forward and backward propagating waves in the interface k. The propagating waves in two consecutive interfaces can be related through the corresponding transfer matrix, that can be obtained multiplying the transfer matrices of a transmission line and a simple reflector:

$$\begin{bmatrix} a_{k+1} \\ b_{k+1} \end{bmatrix} = \begin{bmatrix} e^{-j\theta(\lambda)} & -\rho_k^* e^{-j\theta(\lambda)} \\ -\rho_k e^{-j\theta(\lambda)} & e^{j\theta(\lambda)} \end{bmatrix} \cdot \begin{bmatrix} a_k \\ b_k \end{bmatrix} \qquad (7)$$

The reflection coefficient seen from the first interface ($r_1(\lambda) = b_1(\lambda)/a_1(\lambda)$) is directly the reflection response of the whole structure. For this reason, the starting condition of the layer-peeling algorithm is making $r_1(\lambda)$ equal to the target spectrum. If now we analyze the problem in the time domain, it can be determined that the first sample of the reflection impulse response ($r_1(t = 0)$) must be equal to the reflectivity associated with the first Bragg grating (ρ_1). In other words, ρ_1 can be computed as the zeroth Fourier coefficient (DC component) of $r_1(\lambda)$. Once ρ_1 is calculated, we can manipulate Eq. 7 to obtain the reflection coefficient that has to be seen at the next interface:

$$r_2(\lambda) = e^{j2\theta(\lambda)} \cdot \frac{r_1(\lambda) - \rho_1}{1 - \rho_1^* \cdot r_1(\lambda)}. \qquad (8)$$

With $r_2(\lambda)$ calculated, the reasoning followed before is also valid here, i.e., ρ_2 can be calculated as the zeroth Fourier coefficient of $r_2(\lambda)$ and Eq. 8 can be utilized again to transfer the reflection coefficient to the next interface. Applying iteratively these two steps, the reflectivities ρ_k required for the N Bragg gratings are obtained.

4.- Example of design

4.1.- Definition of the target spectrum

The layer-peeling technique and the proposed Bragg structure can be used to design a filter with a specific spectral response. As a test case, we have chosen a filter with five passbands at arbitrary wavelengths. The target spectrum is determined by defining the modulus of the desired response and windowing its impulse response so that the causality of the filter (null response for $t < 0$) is guaranteed. The size of this window is directly related to both the resemble of the filter with respect to the desired spectrum and the total length of the filter finally designed. For this case, the selected window gives rise to the realizable response shown in Fig. 4, which will be our target from now on.

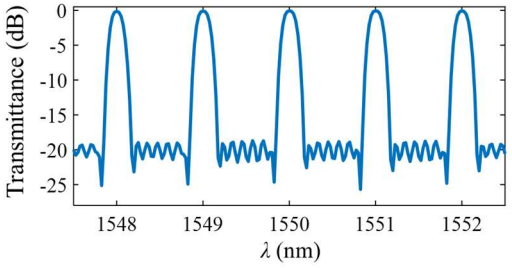

Fig. 4: Target spectrum to be synthesized.

4.2.- Calculation of the gap profile

The defined target spectrum is used as the input for the layer-peeling algorithm. As a result, the algorithm provides a series of discrete reflectivities ρ_k, each of which is going to be synthesized by a single 1-period Bragg grating with gap g_k. The modulus of these reflectivities (Fig. 5(a)) is used in Eq. 4, particularized for $L = \Lambda$ (1-period Bragg grating), to find the coupling coefficient κ required for each grating (Fig. 5(b)). Then, this coupling coefficient can be directly mapped to the corresponding gap g_k through the curve obtained in Fig. 2(f). This way, we obtain the gap apodization profile that implements the target spectrum (Fig. 5(c)).

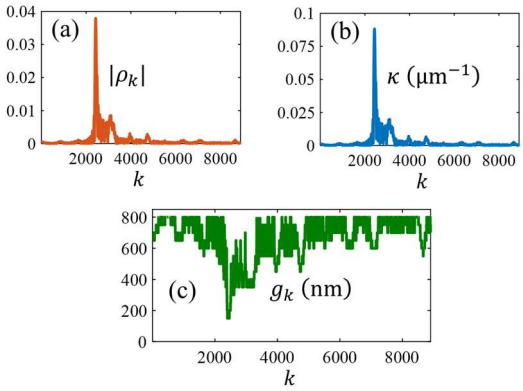

Fig. 5: (a) Modulus of the discrete reflectivities provided by the layer-peeling algorithm. (b) According coupling coefficient. (c) Required gap profile between the central waveguide and the loading segments to synthesize the desired filter response.

4.3.- Calculation of the distance between consecutive loading segments

The calculation of the required gap profile has been performed by uniquely using the modulus of each reflectivity, but there is also a phase term to be taken into. During the layer-peeling process, the electrical length of the different transmission lines (Eq. 6) was selected so that the Bragg wavelength remains constant ($\lambda_B = 1543$ nm). This means that, in principle, each Bragg reflector k should have a nominal period $\Lambda_{\mathrm{nom},k}$ resulting from using its gap g_k in the curve of Fig. 2(d). In that case, the Bragg condition is accomplished. That is to say, the waves reflected at the beginning and at the end of the period interfere constructively. So, the phase shift corresponding to two consecutive reflectivities, $\Delta\phi_k$, would be 0. Nevertheless, if an arbitrary phase shift $\Delta\phi_k = \angle\rho_{k+1} - \angle\rho_k$ is required, the period size of the Bragg reflector k has to be modified as follows:

$$\Lambda_k = \Lambda_{\mathrm{nom},k} \cdot \left(1 - \frac{\Delta\phi_k}{2\pi}\right). \qquad (9)$$

Considering that the length of the segments is going to be maintained (l_b), the variations in the period size are translated into changes of the distance between segments d_k, as is shown in Fig. 1. That is:

$$d_k = \Lambda_k - l_b. \qquad (10)$$

Therefore, by using Eq. 9 and 10, the required phase shift $\Delta\phi_k$ profile shown in Fig. 6(a) results into the distance between segments d_k profile shown in Fig. 6(b).

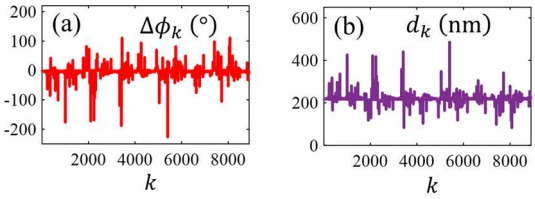

Fig. 6: (a) Required phase shift profile between two consecutive reflectivities. (b) Resultant distance between two consecutive loading segments.

4.4.- Simulation and results

Finally, the complete filter with the corresponding apodization profiles in the gap (Fig. 5(c)) and in the distance between loading segments (Fig. 6(c)) is simulated. In order to avoid 3D simulations that imply an excessive computational effort (the final device is ~3.8 mm long), we have used again our 2D simulation tool [16]. The simulated response is shown in Fig. 7 together with the initial target. The different bands are totally recognizable, and the bandwidth of all of them is practically the same. Likewise, in both cases

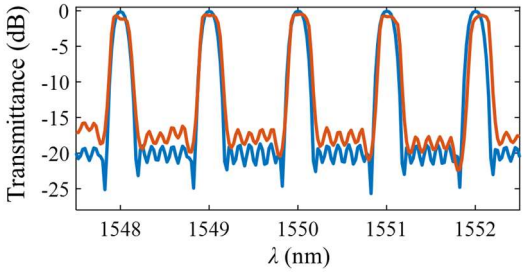

Fig. 7: Simulated transmittance (red) and initial target (blue).

the extinction ratios are higher than 14 dB and the insertion losses at the passbands are around −1 dB. These losses arise from the radiation generated in the multiple discontinuities of the filter that the gap apodization profile imposes. Despite them, we could say that the agreement between both spectra is excellent.

5.- Conclusions

SOI-based Bragg gratings with highly controllable coupling coefficients can be implemented by judiciously placing small segments of silicon within the evanescent field region of a photonic wire waveguide. An optical filter with any desired spectral response can be synthesized by introducing a variation profile in the gap between the central waveguide and the loading segments, as well as in the distance between two consecutive segments. The required apodization profiles can be determined in a straightforward way by using the layer-peeling algorithm, together with a proper electromagnetic analysis of one Bragg period. Our simulations show a good agreement between the synthesized filter and the initial target. We expect that these filters can be implemented in the practice with fabrication tolerances higher than those based on sidewall corrugations.

Ackowledgements: This work has been funded by the Spanish Ministerio de Ciencia, Innovación y Universidades (MICINN) (FPU17/00638, FPU16/06762, TEC2016-80718-R,) and the Universidad de Málaga.

References

[1] David THOMSON, et al., *"Roadmap on silicon photonics"*, Journal of Optics, vol. 18, no. 7, pp. 073003, 2016.

[2] Somnath PAUL, et al., *"Multi-wavelength filtering with a wavegide integrated phase-modulated Bragg grating"*, Optics letters, vol. 42, no. 22, pp. 4635-4638, 2017.

[3] Saket KAUSHAL, et al., *"Optical signal processing based on silicon photonics waveguide Bragg gratings: review"*, Frontiers of Optoelectronics, vol. 11, no. 2, pp. 163-188, 2018.

[4] Ian W. FRANK, et al., *"Nearly arbitrary on-chip optical filters for ultrafast pulse shaping"*, Optics express, vol. 22, no. 19, pp. 22403-22410, 2014.

[5] Kenneth O. HILL, Gerald MELTZ, *"Fiber Bragg Grating technology fundamentals and overview"*, Journal of lightwave techonlogy, vol. 15, no. 8, pp. 1263-1276, 1997.

[6] Johannes SKAAR, et al., *"On the synthesis of Fiber Bragg Gratings by Layer Peeling"*, IEEE Journal of Quantum Electronics, vol. 37, no. 2, pp. 165-173, 2001.

[7] Xu WANG, et al., *"Uniform and sampled Bragg gratings in SOI strip waveguides with sidewall corrugation"*, IEEE Photonics Technology Letters, vol. 23, no. 5, pp. 290-292, 2011.

[8] Xu WANG, et al., *"Narrow-band waveguide Bragg gratings on SOI wafers with CMOS-compatible fabrication process"*, Optics express, vol. 20, no. 14, pp. 15547-15558, 2012.

[9] Alexandre D. SIMARD, et al., *"Apodized Silicon-on-Insulator Bragg gratings"*, IEEE Photonics Technology Letters, vol. 24, no. 12, pp. 1033-1035, 2012.

[10] Rui CHENG, Lukas CHROSTOWSKI, *"Multichannel photonic Hilbert transformers based on complex modulated integrated Bragg gratings"*, Optics letters, vol. 43, no. 5, pp. 1031-1034, 2018.

[11] Rui CHENG, et al., *"Apodization profile amplification of silicon integrated Bragg gratings through lateral phase delays"*, Optics letters, vol. 44, no. 2, pp. 435-438, 2019.

[12] Yung-Jr HUNG, et al., *"Narrowband reflection from weakly coupled cladding-modulated Bragg gratings"*, IEEE Journal of Selected Topics in Quantum Electronics, vol. 22, no. 6, pp. 218-224, 2016.

[13] Jiří ČTYROKÝ, et al., *"Design of narrowband Bragg spectral filters in subwavelength grating metamaterials waveguides"*, Optics express, vol. 26, no. 1, pp. 179-194, 2018.

[14] Pavel CHEBEN, et al., *"Bragg filter bandwidth enginerring in subwavelength grating metamaterial waveguides"*, Optics letters, vol. 44, no. 4, pp. 1043-1046, 2019.

[15] Chin-Lin CHEN, *"Foundations for guided-wave optics"*, (John Wiley & Sons, 2006).

[16] Luis ZAVARGO-PECHE, et al., *"Fourier based combined techniques to design novel sub-wavelength optical integrated devices"*, Progress In Electromagnetics Research, vol. 123, pp. 447-465, 2012.

Other:

(Check the boxes by double-cliking and selecting activate)

☒ I wish to present this communication as candidate for a student prize (only if the first author is a student; they must prove their status as such by an official document which should be sent to optoel2019@unizar.es).

In this case, remember to check the **YES** checkbox in the corresponding form question.